Insight into the Structure of Light-Harvesting Complex II and Its Stabilization in Detergent Solution

Mateus B. Cardoso, Dmitriy Smolensky, William T. Heller,* and Hugh O'Neill*

Center for Structural Molecular Biology, Chemical Sciences Division, Oak Ridge National Laboratory, Oak Ridge, Tennessee 37831

Received: May 29, 2009; Revised Manuscript Received: November 2, 2009

The structure of spinach light-harvesting complex II (LHC II), stabilized in a solution of the detergent *n*-octyl-*β*-D-glucoside (BOG), was investigated by small-angle neutron scattering (SANS). Physicochemical characterization of the isolated complex indicated that it was pure (>95%) and also in its native trimeric state. SANS with contrast variation was used to investigate the properties of the protein−detergent complex at three different H_2O/D_2O contrast match points, enabling the scattering properties of the protein and detergent to be investigated independently. The topological shape of LHC II, determined using ab initio shape restoration methods from the SANS data at the contrast match point of BOG, was consistent with the X-ray crystallographic structure of LHC II (Liu et al. *Nature* **2004** *428*, 287−292). The interactions of the protein and detergent were investigated at the contrast match point for the protein and also in 100% D_2O. The data suggested that BOG micelle structure was altered by its interaction with LHC II, but large aggregate structures were not formed. Indirect Fourier transform analysis of the LHC II/BOG scattering curves showed that the increase in the maximum dimension of the protein−detergent complex was consistent with the presence of a monolayer of detergent surrounding the protein. A model of the LHC II/BOG complex was generated to interpret the measurements made in 100% D_2O. This model adequately reproduced the overall size of the LHC II/BOG complex, but demonstrated that the detergent does not have a highly regular shape that surrounds the hydrophobic periphery of LHC II. In addition to demonstrating that natively structured LHC II can be produced for functional characterization and for use in artificial solar energy applications, the analysis and modeling approaches described here can be used for characterizing detergent-associated α-helical transmembrane proteins.

1. Introduction

Light-harvesting complex II (LHC II) is the most abundant membrane protein in the plant chloroplast and contains approximately 50% of the total chlorophyll (Chl) in the thylakoid membrane.[1] Its primary role is to harvest and transfer solar energy to the reaction center of photosystem II through a Förster-type excitation energy transfer mechanism.[2] In addition to its light-harvesting role, LHC II maintains the supramolecular organization in the thylakoid membranes[3] by inducing the separation and stacking of grana.[4−6] The complex also regulates photosynthesis by dissipating excess excitation energy and controlling energy distribution between photosystems I and II.[7,8]

Native LHC II occurs as a heterotrimeric complex[9,10] composed of lhcb1, lhcb2, and lhcb3 subunits with a stoichiometry of approximately 7:2:1.[9,10] Functional LHC II trimers are typically isolated and purified by partial solubilization of thylakoid membranes using mild detergents, such as Triton X-100, *n*-octyl-*β*-D-glucoside (BOG), and *n*-dodecyl-*β*-D-maltoside, which is retained to stabilize the protein in solution for characterization studies.[11−17] The structures of LHC II variants from pea and spinach have been resolved by X-ray crystallography at 2.5 Å and 2.72 Å, respectively.[18,19] Each subunit of the monomeric polypeptide chain is composed of ∼232 amino acids with 3 membrane-spanning helices that bind and orient 14 Chl and 4 carotenoids. These studies have unambiguously identified the position and orientation of the 8 Chl a, 6 Chl b and 4 carotenoids per monomer.

A combination of spectroscopic studies[11,12,15,20,21] of the detergent-solubilized LHC II trimers and structural information from X-ray crystallographic analysis has provided insight into the mechanisms of trapping, transfer, and dissipation of excitation energy by this protein complex. However, these investigations do not provide direct structural information about the properties of isolated LHC II complexes stabilized in detergent solution, which may differ from its native environment due to the absence of the lipid bilayer and protein−protein interactions that occur therein. Furthermore, protein−detergent interactions are known to influence the structure of membrane proteins in solution, sometimes resulting in structures that deviate from those determined by crystallographic techniques.[22−26]

Small-angle neutron scattering (SANS) with contrast variation is a powerful tool for probing protein−detergent complexes in solution. The difference in the scattering lengths of deuterium and hydrogen makes it possible to highlight individual components of a multicomponent system by varying the ratio of H_2O and D_2O in the solvent. This approach has been applied to a large number of complex systems (e.g., polymer-coated particles,[27,28] self-assembled surfactants,[29,30] block copolymer structures,[31,32]) as well as biological systems.[33−35] In addition, quantitative modeling of SANS data collected at specific contrast match points facilitates understanding of structural changes driven by interactions between the different components of the system. Protein−detergent complexes are ideal candidates for study by SANS with contrast variation because proteins and

* Corresponding authors. (H.O'N.) Phone: 865-574-5004. Fax: 865-574-1275. E-mail: oneillhm@ornl.gov. (W.T.H.) Phone: 865-241-0093. Fax: 865-574-6268. E-mail: hellerwt@ornl.gov.

10.1021/jp905050b
Published on Web 12/02/2009

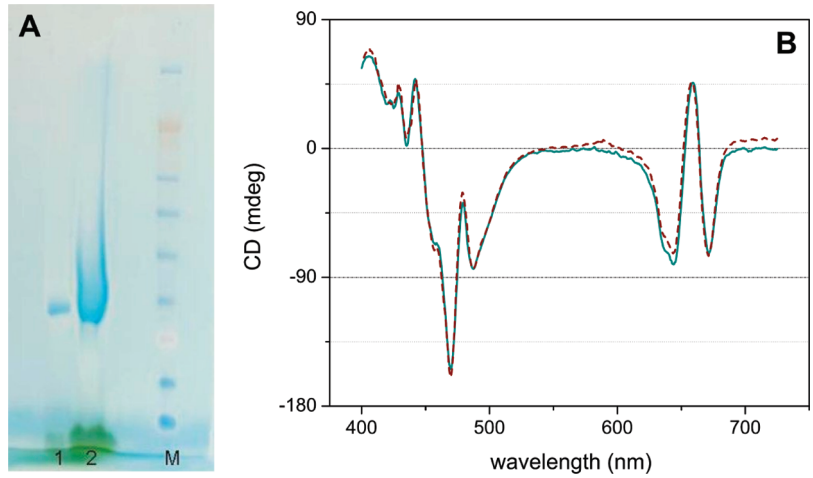

Figure 1. A: SDS PAGE analysis of the LHC II purified from spinach leaves. Lane 1, 9 μg Chl; lane 2, 90 μg Chl; lane M, molecular mass markers. B: Circular dichroism spectra of LHC II samples dissolved in 10 mM Tris HCl pH 7.6, 1.8% (w/v) BOG or the same buffer solution prepared in D_2O (pD 7.6). The dashed red line is the H_2O sample (0.38 mg Chl/mL); the full green line is the spectrum of the D_2O sample (0.34 mg Chl/mL).

detergents have inherently different scattering length densities, making contrast variation possible without isotopic labeling of the sample.

In this study, we report the first SANS investigation of the properties of LHC II stabilized in solution by the detergent BOG. Spectrophotometric and circular dichroism analyses indicated that the protein was in its native conformation under the conditions used for the scattering experiments. By using SANS with contrast variation, the scattering characteristics of the protein in the absence and presence of the scattering contribution of the detergent were separated. The low-resolution shape of the protein was restored from the SANS data at the BOG contrast match point and was found to agree with the crystal structure of spinach LHC II.[19] The interactions of the protein and detergent were investigated at the contrast match point for the protein and also in 100% D_2O. A structural model built of the LHC II/BOG complex indicates that the belt of detergent surrounding LHC II trimer is not consistent with a highly regular structure encompassing the protein. This study gives insight into the solution properties of LHC II trimers. In addition, the characterization approaches described will have broader application in the investigation of α-helical transmembrane protein−detergent interactions.

2. Material and Methods

2.1. Isolation of LHC II. Market spinach leaves were coarsely ground (<2 mm) using a food processor, followed by homogenizing with two volumes of 50 mM Tricine−KOH pH 7.8 and 0.4 M sorbitol in a commercial blender for 30 s. The suspension was filtered through 8 layers of cheese cloth and centrifuged at 10000*g* for 10 min. The pellet was resuspended in 20 mM Tricine/KOH pH 7.8, 5 mM EDTA, and 50 mM sorbitol using a Potter homogenizer to disperse large membrane aggregates, followed by centrifugation at 10000*g* for 10 min. The thylakoid membranes were resuspended in 20 mM Tricine/KOH pH 7.8 as described above, and the Chl concentration was adjusted to 0.8 mg/mL.[36] LHC II was selectively released from the thylakoid membranes by addition of Triton X-100 to a final concentration of 0.9% (w/v) (from a 10.5% (w/v) stock, CalBiochem, sterile protein grade). The sample was stirred on an ice bath for 45 min, followed by centrifugation at 30000*g* for 40 min. The supernatant was applied to a continuous sucrose gradient (0.1−1.0 M) that contained 20 mM Tricine and 0.05% (w/v) Triton X-100 and centrifuged at 26000 rpm in a SW28 rotor for 18 h. After centrifugation, two Chl-containing bands were observed. The top band (upper portion of the gradient) contained the LHC II, and the lower one consisted of larger membrane fragments and photosystem I.[24] The LHC II band was removed, and $MgCl_2$ and KCl were added to a final concentration of 25 mM and 150 mM, respectively. The solution was stirred for 15 min on an ice bath and centrifuged at 30000*g* for 45 min to precipitate the LHC II complexes. The pellets were recovered, dissolved in 10 mM Tris−HCl buffer pH 7.6 containing 1.8% (w/v) BOG, and stored at 4 °C.

2.2. Analytical Procedures. For characterization studies, the Chl content was determined in 80% acetone according to procedures described in the literature.[37] Protein concentration was calculated on the basis of the known Chl content of LHC II (eight Chl *a* and six Chl *b* per monomer). Circular dichroism spectra were recorded on a Jasco 810 circular dichroism spectropolarimeter at 25 °C. The purity of the LHC II was assessed by denaturing SDS−PAGE electrophoresis performed using 12% acrylamide gels (ClearPAGE, CBS Scientific). The molecular mass markers were SeeBlue Plus2 (CBS Scientific).

2.3. Small-Angle Neutron Scattering Data Collection. SANS experiments were carried out using the Bio-SANS instrument[38] at the High Flux Isotope Reactor of Oak Ridge National Laboratory. Scattering data were recorded for scattering vectors (q) $0.009 < q < 0.19$ Å^{-1} ($q = (4\pi/\lambda)\sin(\theta/2)$, λ is the neutron wavelength and θ is the scattering angle) using 6 Å neutrons with a wavelength spread, $\Delta\lambda/\lambda$, of 0.15. Data were collected using a 0.4 m × 0.4 m position-sensitive He^3 detector (Ordela, Inc., Oak Ridge, TN) at sample-to-detector distances of 1.1 and 6.8 m. The center of the detector was offset 150 mm from the beam.

For SANS analysis, the samples were prepared by resuspending the LHC II pellets obtained from the final purification step in 10 mM Tris HCl pH 7.6 containing 1.8% (w/v) BOG or the same buffer solution prepared in D_2O (pD 7.6). The LHC II samples were mixed to obtain final D_2O concentrations of 15.0, 42.0, and 100.0% D_2O with final protein concentrations of 3.95, 4.17, and 4.65 mg/mL, respectively. The appropriate buffer solutions without protein were also collected for use in the data reduction. SANS measurements were carried out at room temperature in 1.0 mm path quartz cuvettes. The raw data were

corrected for detector sensitivity, solvent background, and transmission.

2.4. SANS Data Analysis and Modeling. The small-angle scattering from a dilute solution of particles can be written as

$$\frac{d\sigma(q)}{d\Omega(q)} = n\Delta\rho^2 V^2 P(q) S(q) \quad (1)$$

where n is the number density of particles, $\Delta\rho$ is the difference in scattering density between the particles and the solvent, V is the volume of the particle, $P(q)$ is the form factor, and $S(q)$ is the structure factor. $P(q)$ is a function of the size and shape of the scattering particles in the sample that is averaged over all orientations relative to the incident beam. The effective structure factor, $S(q)$, provides information about the interparticle interactions and for dilute solutions of noninteracting particles, $S(q) = 1$.

The radius of gyration (R_g) for the protein experimental scattering curve was evaluated by using the Guinier approximation[39]

$$I(q) = I(0)\, e^{-q^2 R_g^2/3} \quad (2)$$

where $I(0)$ is the forward scattering, which is a shape-independent function of the total scattering power of the sample. By performing a linear fit to a $\ln(I(q))$-vs-q^2 plot (commonly called Guinier plot), $I(0)$ and R_g can be determined from the intercept and slope, respectively. The distance distribution function, $p(r)$, and particle maximum dimension, D_{max}, were determined by fitting the data using the indirect Fourier transform method implemented in the program GNOM.[40]

The form factor $P(q)$ of a cylinder of length L and radius r is given by eq 3.[41]

$$P(q) = \int_0^{\pi/2} \left[\frac{2J_1(qr\sin\alpha)}{qr\sin\alpha}\frac{\sin((qL\cos\alpha)/2)}{(qL\cos\alpha)/2}\right]^2 \sin\alpha\, d\alpha \quad (3)$$

J_1 is the first-order Bessel function, and α is the variable of integration. The effect of radius polydispersity can be accounted for by convoluting $P(q)$ with a Schultz distribution, shown in eq 4

$$f(r) = \frac{r^z}{\Gamma(z+1)}\left[\frac{z+1}{r_{avg}}\right]^{z+1} \exp\left(-\frac{(z+1)r}{r_{avg}}\right) \quad (4)$$

where, $\Gamma(n)$ is the gamma function and z is the polydispersity parameter defined by

$$z = \left(\frac{r_{avg}}{\sigma_r}\right)^2 - 1 \quad (5)$$

Data fitting was performed using Igor software routines developed at the National Institutes of Standards and Technology.[42] The quality of the fit to the data was evaluated with the reduced χ^2 parameter.[43]

Reconstruction of the low-resolution shape of LHC II from the data collected in 15% D_2O was performed using the program DAMMIF.[44] For shape reconstruction of trimeric LHC II, $P3$ symmetry was applied to the models, which were assumed to be oblate in shape. Fifty runs of DAMMIF were performed, and the resulting set of models were used to determine the average structure using the program DAMAVER.[45] Direct comparison of the experimental LHC II curve with the profile calculated from the crystal structure of the LHC II trimer[19] was accomplished using the program ORNL_SAS.[46]

To model the SANS data collected in 100% D_2O, the contributions from the detergent-associated LHC II and the free micelles had to be taken into account. Structural models utilizing the high-resolution structure of LHC II[19] were generated using a previously applied approach.[25] Briefly, a discoidal structure is generated having a radius R and a half-thickness T (see Figure 1 of reference[25]). The core of this structure, being the hydrophobic core, has a half-thickness C. The outer edge of the disk is the outer edge of a torus with the same core−shell structure as the planar disk. The resulting structure has a contiguous shell in which the upper and lower outer shells of the structure are part of a single volume that has a thickness $T - C$. The entire detergent structure is then superimposed onto the high-resolution structure such that the remaining discoidal structure encompasses the transmembrane domain of the protein, leaving a beltlike detergent structure around the membrane protein. Intensity profiles of LHC II/BOG complexes were calculated for a series of detergent disk radii. On the basis of the previous work, the value of T was set to 15 Å,[25] and C was set to 10.5 Å, giving a shell thickness of 4.5 Å.[47] Both parameters were fixed to minimize the number of free parameters involved in the model fit to the data. The LHC II/BOG complex structure that presented an average detergent belt of around 15 Å, resulting from R of 35 Å, was chosen on the basis of the results of the $p(r)$ fitting for use in the remainder of the modeling. The scattering intensity pattern was simulated at 100% D_2O using ORNL_SAS software.[46] The intensity profile of the free BOG micelles was calculated taking into account a cylindrical model with polydispersity applied to the radius using parameters resulting from the fitting of the SANS data collected at 100% D_2O. The BOG micelle scattering profile was simulated using the Igor software routine.[42] Then, linear superpositions of the two profiles, scaled to unity at $q = 0$, were generated according to eq 6,

$$I_{tot}(q) = AI_{LHCII}(q) + BI_{MIC}(q) \quad (6)$$

where $I_{LHCII}(q)$ is the profile calculated from the crystal structure in the detergent belt and $I_{MIC}(q)$ is the calculated intensity profile of the free micelles. A and B are the mixing constants and range from 0 to 1 with the constraint that $A + B = 1$. A global scaling constant was also applied for comparing $I_{tot}(q)$ to the SANS data. The parameters A and B are related to the number of LHC II/BOG complexes and free micelles.

3. Results

3.1. Physicochemical Properties of the LHC II Preparation. LHC II was isolated from spinach thylakoids by solubilizing the membranes with Triton X-100 detergent. The solubilized membranes were fractionated by density gradient ultracentrifugation over a continuous 0.1−1.0 M sucrose gradient. After centrifugation, the band containing LHC II was removed and separated from free Chl by Mg^{2+}/K^+ cation-induced appression. The yield of LHC II was ~11.5 mg from 300 g of starting material. The Chl *a*-to-Chl *b* ratio was found to be 1.28, which is similar to values reported previously.[21,37,48] Analysis of the purified protein by SDS−PAGE revealed a single band with a molecular mass of ~25 kDa (Figure 1A, lane 1). Application of 10 times the amount of protein to the gel showed that no major contaminating proteins were present in the sample (Figure 1A, lane 2).

The circular dichroism (CD) spectrum of LHC II in the visible region is very sensitive to pigment−pigment interactions and can distinguish between monomeric and trimeric LHC II. For CD measurements, the LHC II samples in 100% H_2O and 100% D_2O were diluted into the appropriate buffered solution contain-

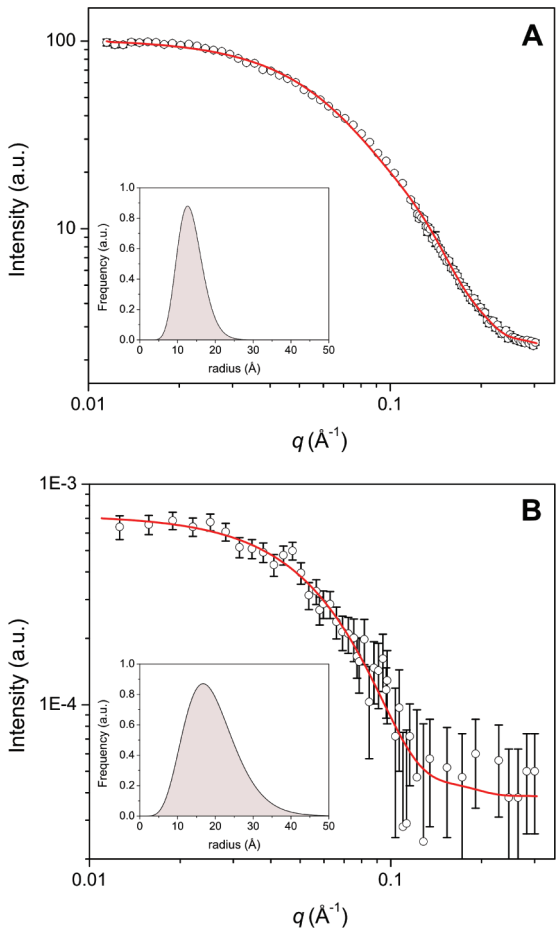

Figure 2. SANS analysis of BOG data obtained in (A) 100% D_2O solution and (B) in LHC II solution with 42% D_2O. The solid red line represents the polydisperse radius cylindrical fit. Inset plots show the distributions of the radii of the cylinders for each sample determined by the fitting.

ing 1.8% BOG detergent, and the spectra were recorded within 5 min. The spectra overlay well, indicating that the presence of D_2O does not significantly alter the structure of the complex (Figure 1B). In the Q_y region of the spectrum, a shoulder is visible at 648 nm that is not present in monomeric LHC II.[49] In the Soret region, there are two spectral features observed, a prominent negative signal at 478 nm and a broad positive signal at 412 nm, that are present only in LHC II trimers.[50] This gives good confidence that the LHC II is in its trimeric form. CD spectra of LHC II were also recorded 48 h after the SANS measurements (data not shown). Overall, the shapes of the spectra were essentially the same as those published previously for detergent-solubilized LHC II.[50−52]

3.2.1. SANS Analysis of BOG Micelles. SANS measurements were performed to characterize the structure of the BOG in the presence and absence of LHC II. The scattering profile of BOG dissolved in 100% D_2O is shown in Figure 2A. The scattering curve agrees with previously published data.[53] Prolate ellipsoid and cylindrical models have been used in previous studies to fit the SANS profiles of small and large BOG micelles, respectively.[53−56] The data presented here were fit using a cylindrical model with polydispersity applied to the radius. The inset plot of Figure 2A shows the distributions of radii used to produce the fit intensity profile. The parameters resulting from the model fitting of the SANS data are summarized in Table 1. The average cylinder radius (r_{avg} = 13.5 ± 0.3 Å) agrees very well with previously reported values,[53,54] but is less than the

TABLE 1: Structural Parameters Obtained from SANS Data by Polydisperse Radius Cylindrical Model

sample[a]	cylinder average radii, r_{avg} (Å)	σ_r/r_{avg}	length, L (Å)	radius of gyration, R_g (nm)	χ^2
A	13.5 ± 0.3	0.25 ± 0.02	82.5 ± 1.3	25.6 ± 0.4	1.76
B	19.3 ± 9.9	0.36 ± 0.28	53.6 ± 47.2	20.6 ± 15.0	0.69

[a] Sample A = BOG dissolved in 100% D_2O; sample B = LHC II/BOG mixture in 42% D_2O.

length of a fully extended BOG molecule (15.4 Å),[57] suggesting that the hydrocarbon chains are not fully extended or that there is interdigitation of the alkyl chains within the micelles. The length (L) of the micelles was determined to be 82.5 ± 1.3 Å, giving a radius of gyration (R_g) of 25.6 ± 0.4 Å. On the basis of the volume of the cylinder (4.7×10^4 Å^3), the volume of a BOG molecule (418.6 Å^3), and assuming a water-free micelle, the particle would be formed by ~100 BOG molecules. However, it is known that a substantial amount of solvent penetrates into the BOG headgroup region, displacing detergent from the total volume of the micelle,[58] making the number of BOG molecules in the micelle determined here an upper limit.

The experimental scattering profile observed for the LHC II/BOG mixture at 42% D_2O is dominated by the detergent (Figure 2B). The polydisperse cylinder fitting reveals that the diameter increases (r_{avg} = 19.3 ± 9.9 Å) while the length decreases (L = 53.6 ± 47.2 Å). In comparison to the 100% D_2O data, the greatly reduced contrast between the BOG and buffer at 42% D_2O has reduced the signal-to-noise ratio and significantly increased the experimental uncertainty, which in turn impacts the reliability of the fitting. In addition, the micelle size and shape inferred by fitting the scattering data cannot be considered unique or rigorous because the scattering profile corresponds to a mixture between BOG micelles and BOG associated with LHC II. The presence of detergent-unfolded LHC II is excluded, since the scattering data for the LHC II/BOG samples do not show a power-low scattering consistent with correlated particles.[24,25] Rather, the data are consistent with the presence of relatively compact scattering particles.

3.2.2. SANS Analysis of LHC II. To probe the structure of LHC II in the micelle solution, SANS measurements were carried out in 15% D_2O, near the contrast match point for BOG micelles (Figure 3).[57] As expected, the counting statistics at high q values were poor as a result of the relatively low concentration of LHC II in the sample and the low contrast of LHC II in 15% D_2O solution. The Guinier plot[39] of the data, shown in the inset of Figure 3, is linear, giving an R_g of 28.3 ± 1.6 Å. The $p(r)$ determined using GNOM[40] is shown in Figure 4, whereas the fit curve is shown with the data in Figure 3. Its shape is similar to the asymmetric $p(r)$ curves previously reported for membrane proteins.[24,26,59] The curve has a main peak at ~36 Å that decays with a small tail to a maximum particle size, D_{max}, of 80 ± 5 Å, as determined by varying D_{max} between 75 and 85 Å during the $p(r)$ fitting. A second measure of R_g is provided by the second moment of the $p(r)$ function, being 28.4 ± 1.7 Å, in good agreement with the value determined by Guinier fitting. The agreement of the data with the scattering intensity profile calculated from the crystal structure of LHC II[19] was evaluated using ORNL_SAS,[46] and is shown in Figure 3. The model profile fits the data well, and the R_g calculated from the simulated scattering profile, 28.3 Å, is in agreement with the experimentally determined value. The scattering of a LHC II monomer was also simulated (not shown), but it did not fit the experimental data. To better understand the structure of the LHC II,

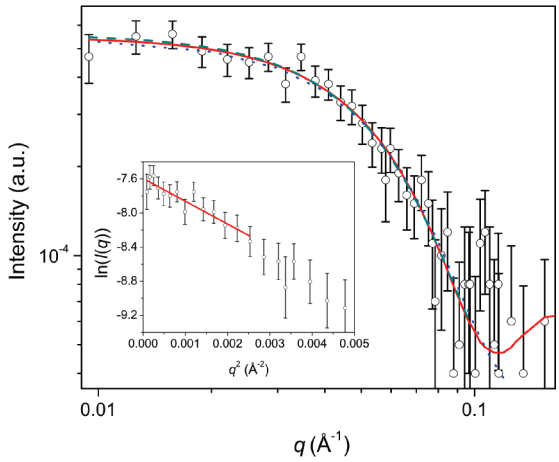

Figure 3. SANS data of LHC II/BOG mixture dissolved in 15% D_2O (○). Theoretical scattering profile of LHC II crystal structure is presented as the solid red line, GNOM fit is the dashed green line, and the ab initio model fit is the blue dotted line. The inset represents the Guinier plot of ln($I(q)$) vs q^2 of the scattering intensity profile of LHC II.

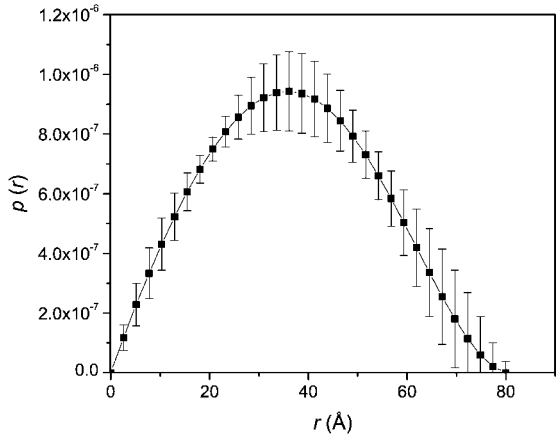

Figure 4. Pair distance distribution function $p(r)$ obtained from the indirect Fourier transform method of the LHC II/BOG mixture dissolved in 15% D_2O.

shape restoration was performed using the software DAMMIF[44] using q-values ≤0.1 Å^{-1}. The average structure from multiple runs of the program using a constraint of $P3$ symmetry was determined by the DAMAVER program.[45] SUPCOMB[60] was used to superimpose the restored envelope onto the crystal structure of LHC II[19] (Figure 5). Interestingly, there is a region of lower electron density evident in the center of the consensus model that is occupied by a phosphatidylglycerol lipid moiety in the LHC II crystal structure. In a 15% D_2O solution, the scattering length density of the lipid will be nearly matched to that of the solvent, resulting in an effective hole in the structure. Therefore, additional tests were performed during the modeling by applying hollow oblate cylinders to enforce the presence of a hole in the center for the restored envelope or solid oblate cylinders to enforce the absence of the hole. The overall shapes and sizes of the restored envelopes were not impacted by enforcing the presence of the hole. As can be seen in Figure 5, the consensus structure resulting from multiple, independent runs of the shape restoration agrees with the shape of the crystal structure of LHC II.[19] Comparison of the lateral view of the restored envelope superimposed onto the crystal structure (Figure 5C) shows that their respective heights are slightly different. A similar observation was reported in a study that

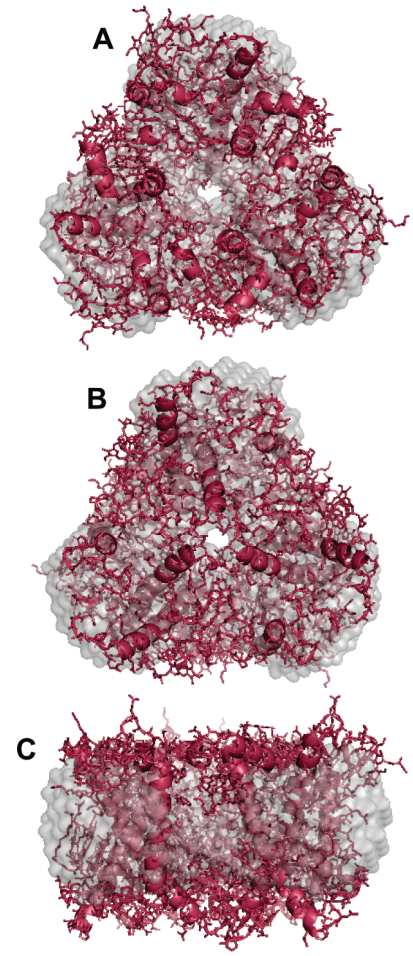

Figure 5. Comparison of restored low-resolution structural model (gray) and high-resolution LHC II crystal structure (red). A, top view; B, bottom view; and C, lateral view. Top and bottom views were arbitrarily chosen.

investigated ab initio shape reconstruction of the bacterial light-harvesting complex (LH2) from its X-ray scattering profile.[26,61]

3.2.3. The Interaction of LHC II and BOG. Unlike the SANS measurements of the LHC II/BOG mixture made in 15 and 42% D_2O, the SANS profile for the LHC II/BOG micelle sample measured in 100% D_2O, shown in Figure 6, results from free micelles and LHC II/BOG complexes. The data have a linear Guinier region (not shown), giving a R_g of 31.2 ± 0.1 Å, indicating that the samples are free of large aggregates. The $p(r)$ curve derived from the data is shown in Figure 7; the profile resulting from the fitting is shown with the data in Figure 6. The $p(r)$ has a peak at 30 Å that decays monotonically to a D_{max} of 110 ± 10 Å. The R_g calculated from the $p(r)$ function is 32.4 ± 0.2 Å. Comparison of the $p(r)$ analysis of the LHC II/BOG mixtures in 15% and 100% D_2O with the $p(r)$ derived for BOG in 100% D_2O, shown together in Figure 7, reveals important differences. The $p(r)$ of LHC II/BOG in 100% D_2O appears to be intermediate in shape between the $p(r)$ of LHC II structure and that of the cylindrical BOG micelles. The LHC II/BOG with free BOG micelles measured in 100% D_2O has a D_{max} 30 Å larger than when the BOG is contrast-matched out at 15% D_2O, approximately twice the length of a single BOG molecule (~15 Å). The results support the presence of BOG around the longest dimension of the LHC II structure, which is indicated to be the edge of the flattened dimension of the oblate structure, and is consistent with the membrane-spanning surface of the LHC II crystal structure.[19] This interpretation is in

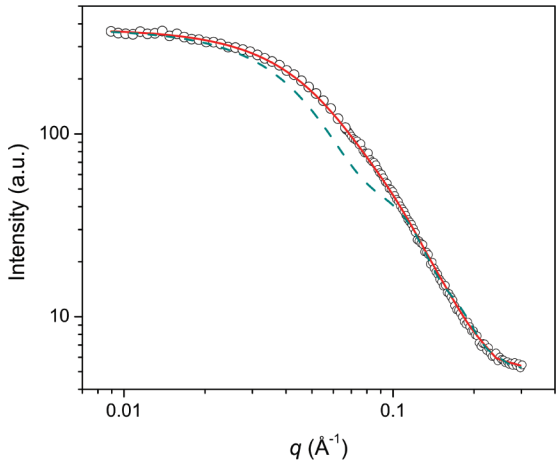

Figure 6. SANS data (○) obtained from the LHC II/BOG mixture in 100% D_2O. Solid red line represents the fit obtained through GNOM program. Dashed green line is the curve fit obtained from the linear superposition between the fit of BOG micelles in 100% D_2O and the simulated scattering pattern generated through the LHC II/BOG belt model.

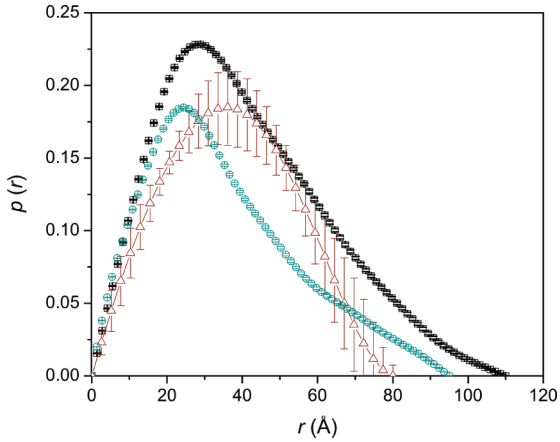

Figure 7. Pair distance distribution function $p(r)$ obtained from LHC II/BOG mixture in 15% (red triangles) and 100% D_2O (black squares) as well as BOG micelles in 100% D_2O (green circles).

agreement with previous investigations on membrane protein−detergent interactions. In these studies, it was determined that a monolayer ring is the most likely structure of detergent that is bound to membrane proteins, rather than the proteins embedded in preformed micelles.[22,62−66]

A model was generated such that the LHC II was embedded in a detergent disk that surrounded the hydrophobic part of the protein (shown in Figure 8A and B), as described previously.[25] An ∼15 Å detergent layer surrounding the protein was considered so as to increase the total D_{max} by ∼30 Å, to obtain the same maximum particle dimension observed in the scattering profile of LHC II/BOG mixture in 100% D_2O. The upper limit of BOG molecules in the detergent belt shown in Figure 8, having a volume of 1.8×10^5 Å^3 and considering solvent penetration into the BOG headgroup region,[58] is ∼440, or approximately four times the estimated aggregation number determined for the protein-free BOG micelles.

Modeling the protein−detergent complex using the experimental data is complicated by the presence of free detergent micelles. Therefore, a function was generated that consists of a superposition of the cylinder form factor for a BOG micelle and the theoretical scattering curve of LHC II embedded in a detergent disk. The best fit line, shown in Figure 6, corresponds

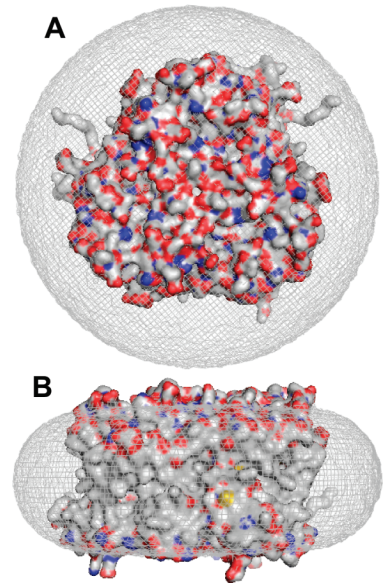

Figure 8. Superior (A) and lateral (B) views of LHC II protein surface embedded in a disklike detergent micelle belt (gray meshed region around the protein). Carbon atoms are gray, and nitrogen atoms and oxygen atoms are blue and red, respectively.

to a convolution in which the ratio of free micelles to the protein detergent disk is ∼1:4, in agreement with the BOG concentration used to dissolve the protein. The fit curve reproduces the experimental scattering signature well at low- and high-q values but deviates from the experimental data in the mid-q range. The observed discrepancy between the model and experimental scattering profiles is a scattering minimum at ∼0.07 Å^{-1} and results from the uniform geometric shape of the LHC II/BOG belt model. The absence of the minimum in the experimental data could be due to a nonuniform shape of the BOG around the protein and suggests that the idealized geometry of the detergent disk encapsulating the hydrophobic part of the protein used here is a simplification that does not accurately reflect the interaction of BOG with LHC II trimers. One possibility is an interdigitation of the alkyl chains of BOG into the α-helices of LHC II, which has been previously observed for other membrane proteins surrounded by lipid molecules in their native environment.[67]

Conclusions

The results of this SANS study provide important insights into properties of spinach LHC II in solution. Using SANS with contrast variation, it was possible to extract the scattering signature of LHC II at the contrast match point of the detergent. The shape of the scattering curve was consistent with the expected profile of trimeric LHC II. The ab initio shape restoration confirmed that the low-resolution molecular envelope of the protein is consistent with the structural features of the X-ray crystallographic structure of spinach LHC II trimers. Indirect Fourier transform analysis of the scattering curves of LHC II with and without the scattering contribution of detergent indicated that the difference in the maximum dimension of the protein−detergent complex was consistent with the presence of a monolayer of detergent surrounding the protein. A model, representing a disk of detergent surrounding the hydrophobic portion of LHC II, was constructed. This model adequately described the overall size of the LHC II/BOG complex, but it also showed that the detergent does not have a highly regular shape that encompasses the hydrophobic periphery of LHC II.

The analysis and modeling approaches described here may have broader implications for investigation of the interaction of detergents with α-helical transmembrane proteins.

Acknowledgment. M.B.C. thanks Capes-Brazil for the support. This work was supported by the ORNL Laboratory Director's Research Development Program. This research at Oak Ridge National Laboratory's Center for Structural Molecular Biology (CSMB) was supported by the Office of Biological and Environmental Research, using facilities supported by the U.S. Department of Energy, managed by UT-Battelle, LLC, under Contract No.DE-AC05-00OR22725.

References and Notes

(1) Kuhlbrandt, W.; Wang, D. N.; Fujiyoshi, Y. *Nature* **1994**, *367*, 614.
(2) Forester, T. *Discuss. Faraday Trans.* **1959**, *27*, 7.
(3) Zhang, S. P.; Scheller, H. V. *J. Biol. Chem.* **2004**, *279*, 3180.
(4) Mustardy, L.; Garab, G. *Trends Plant Sci.* **2003**, *8*, 117.
(5) Mullet, J. E.; Arntzen, C. J. *Biochim. Biophys. Acta* **1980**, *589*, 100.
(6) Barber, J. *Annu. Rev. Plant Physiol. Plant Mol. Biol.* **1982**, *33*, 261.
(7) Elrad, D.; Niyogi, K. K.; Grossman, A. R. *Plant Cell* **2002**, *14*, 1801.
(8) Horton, P.; Ruban, A. V.; Walters, R. G. *Annu. Rev. Plant Physiol. Plant Mol. Biol.* **1996**, *47*, 655.
(9) Jansson, S. *Biochim. Biophys. Acta, Bioenerg.* **1994**, *1184*, 1.
(10) Caffarri, S.; Croce, R.; Cattivelli, L.; Bassi, R. *Biochemistry* **2004**, *43*, 9467.
(11) Ide, J. P.; Klug, D. R.; Kuhlbrandt, W.; Giorgi, L. B.; Porter, G. *Biochim. Biophys. Acta* **1987**, *893*, 349.
(12) Mullineaux, C. W.; Pascal, A. A.; Horton, P.; Holzwarth, A. R. *Biochim. Biophys. Acta, Bioenerg.* **1993**, *1141*, 23.
(13) Nussberger, S.; Dekker, J. P.; Kuehlbrandt, W.; van Bolhuis, B. M.; van Grondelle, R.; van Amerongen, H. *Biochemistry* **1994**, *33*, 14775.
(14) Kwa, S. L. S.; Groeneveld, F. G.; Dekker, J. P.; van Grondelle, R.; van Amerongen, H.; Lin, S.; Struve, W. S. *Biochim. Biophys. Acta, Bioenerg.* **1992**, *1101*, 143.
(15) Peterman, E. J. G.; Hobe, S.; Calkoen, F.; van Grondelle, R.; Paulsen, H.; van Amerongen, H. *Biochim. Biophys. Acta, Bioenerg.* **1996**, *1273*, 171.
(16) Rogl, H.; Schodel, R.; Lokstein, H.; Kuhlbrandt, W.; Schubert, A. *Biochemistry* **2002**, *41*, 2281.
(17) Wentworth, M.; Ruban, A. V.; Horton, P. *Biochemistry* **2004**, *43*, 501.
(18) Standfuss, R.; van Scheltinga, A. C. T.; Lamborghini, M.; Kuhlbrandt, W. *EMBO J.* **2005**, *24*, 919.
(19) Liu, Z. F.; Yan, H. C.; Wang, K. B.; Kuang, T. Y.; Zhang, J. P.; Gui, L. L.; An, X. M.; Chang, W. R. *Nature* **2004**, *428*, 287.
(20) Lambrev, P. H.; Varkonyi, Z.; Javorfi, T.; Kiss, A.; Namkhainyambuu, B. A.; Szabo, M.; Garab, G. *FEBS J.* **2005**, *272*, 452.
(21) Simidjiev, I.; Barzda, V.; Mustardy, L.; Garab, G. *Anal. Biochem.* **1997**, *250*, 169.
(22) le Maire, M.; Champeil, P.; Moller, J. V. *Biochim. Biophys. Acta, Biomembr.* **2000**, *1508*, 86.
(23) Seddon, A. A.; Curnow, P.; Booth, P. J. *Biochim. Biophys. Acta, Biomembr.* **2004**, *1666*, 105.
(24) O'Neill, H.; Heller, W. T.; Helton, K. E.; Urban, V. S.; Greenbaum, E. *J. Phys. Chem. B* **2007**, *111*, 4211.
(25) Mo, Y.; Lee, B. K.; Ankner, J. F.; Becker, J. M.; Heller, W. T. *J. Phys. Chem. B* **2008**, *112*, 13349.
(26) Hong, X. G.; Weng, Y. X.; Li, M. *Biophys. J.* **2004**, *86*, 1082.
(27) Dingenouts, N.; Seelenmeyer, S.; Deike, I.; Rosenfeldt, S.; Ballau, M.; Lindner, P.; Narayanan, T. *Phys. Chem. Chem. Phys.* **2001**, *3*, 1169.
(28) Hone, J. H. E.; Cosgrove, T.; Saphiannikova, M.; Obey, T. M.; Marshall, J. C.; Crowley, T. L. *Langmuir* **2002**, *18*, 855.
(29) Bagger Jorgensen, H.; Olsson, U.; Mortensen, K. *Langmuir* **1997**, *13*, 1413.
(30) Bumajdad, A.; Eastoe, J.; Heenan, R. K.; Lu, J. R.; Steytler, D. C.; Egelhaaf, S. *J. Chem. Soc. Faraday Trans.* **1998**, *94*, 2143.
(31) Forster, S.; Wenz, E.; Lindner, P. *Phys. Rev. Lett.* **1996**, *77*, 95.
(32) McConnell, G. A.; Lin, E. K.; Gast, A. P.; Huang, J. S.; Lin, M. Y.; Smith, S. D. *Faraday Discuss.* **1994**, 121.
(33) Gau-Racine, J.; Lal, J.; Zeghal, M.; Auvray, L. *J. Phys. Chem. B* **2007**, *111*, 9900.
(34) Mutch, K. J.; van Duijneveldt, J. S.; Eastoe, J.; Grillo, I.; Heenan, R. K. *Langmuir* **2008**, *24*, 3053.
(35) Jeng, U. S.; Lin, T.-L.; Lin, J. M.; Ho, D. L. *Phys. B: Condens. Matter* **2006**, *385*−*386*, 865.
(36) Arnon, D. I. *Plant Physiol.* **1949**, *24*, 1.
(37) Porra, R. J.; Thompson, W. A.; Kriedemann, P. E. *Biochim. Biophys. Acta, Bioenerg.* **1989**, *975*, 384.
(38) Lynn, G. W.; Heller, W.; Urban, V.; Wignall, G. D.; Weiss, K.; Myles, D. A. A. *Phys. B: Condens. Matter* **2006**, *385*−*386*, 880.
(39) Guinier, A.; Fournet, G. *Small-Angle Scattering of X-Rays*; John Wiley & Sons: London, UK., 1955.
(40) Svergun, D. I. *J. Appl. Crystallogr.* **1992**, *25*, 495.
(41) Pedersen, J. S. *Adv. Colloid Interface Sci.* **1997**, *70*, 171.
(42) Kline, S. R. *J. Appl. Crystallogr.* **2006**, *39*, 895.
(43) Taylor, J. R. *An Introduction to Error Analysis: The Study of Uncertainties in Physical Measurements*, 2nd ed.; University Science Book: Sausalito, CA, 1997.
(44) Svergun, D. I. *Biophys. J.* **1999**, *76*, 2879.
(45) Volkov, V. V.; Svergun, D. I. *J. Appl. Crystallogr.* **2003**, *33*, 860.
(46) Tjioe, E.; Heller, W. T. *J. Appl. Crystallogr.* **2007**, *40*, 782.
(47) Lipfert, J.; Columbus, L.; Chu, V. B.; Lesley, S. A.; Doniach, S. *J. Phys. Chem. B* **2007**, *111*, 12427.
(48) Standfuss, J.; Kuhlbrandt, W. *J. Biol. Chem.* **2004**, *279*, 36884.
(49) Hemelrijk, P. W.; Kwa, S. L. S.; van Grondelle, R.; Dekker, J. P. *Biochim. Biophys. Acta, Bioenerg.* **1992**, *1098*, 159.
(50) Hobe, S.; Prytulla, S.; Kuhlbrandt, W.; Paulsen, H. *EMBO J.* **1994**, *13*, 3423.
(51) Ruban, A. V.; Calkoen, F.; Kwa, S. L. S.; vanGrondelle, R.; Horton, P.; Dekker, J. P. *Biochim. Biophys. Acta, Bioenerg.* **1997**, *1321*, 61.
(52) Lambrev, P. H.; Varkonyi, Z.; Krumova, S.; Kovacs, L.; Miloslavina, Y.; Holzwarth, A. R.; Garab, G. *Biochim. Biophys. Acta, Bioenerg.* **2007**, *1767*, 847.
(53) Giordano, R.; Maisano, G.; Teixeira, J. *J. Appl. Crystallogr.* **1997**, *30*, 761.
(54) He, L. Z.; Garamus, V.; Niemeyer, B.; Helmholz, H.; Willumeit, R. *J. Mol. Liq.* **2000**, *89*, 239.
(55) D'Aprano, A.; Giordano, R.; Jannelli, M. P.; Magazù, S.; Maisano, G.; Sesta, B. *J. Mol. Struct.* **1996**, *383*, 177.
(56) He, L.-Z.; Garamus, V. M.; Funari, S. S.; Malfois, M.; Willumeit, R.; Niemeyer, B. *J. Phys. Chem. B* **2002**, *106*, 7596.
(57) Prince, S. M.; Howard, T. D.; Myles, D. A. A.; Wilkinson, C.; Papiz, M. Z.; Freer, A. A.; Cogdell, R. J.; Isaacs, N. W. *J. Mol. Biol.* **2003**, *326*, 307.
(58) Zhang, R. T.; Marone, P. A.; Thiyagarajan, P.; Tiede, D. M. *Langmuir* **1999**, *15*, 7510.
(59) Santonicola, M. G.; Lenhoff, A. M.; Kaler, E. W. *Biophys. J.* **2008**, *94*, 3647.
(60) Kozin, M. B.; Svergun, D. I. *J. Appl. Crystallogr.* **2001**, *34*, 33.
(61) Du, L. C.; Weng, Y. X.; Hong, X. G.; Xian, D. C.; Katsumi, K. *Chin. Phys. Lett.* **2006**, *23*, 1861.
(62) Moller, J. V.; Lemaire, M. *J. Biol. Chem.* **1993**, *268*, 18659.
(63) Roth, M.; Lewitbentley, A.; Michel, H.; Deisenhofer, J.; Huber, R.; Oesterhelt, D. *Nature* **1989**, *340*, 659.
(64) Pebaypeyroula, E.; Garavito, R. M.; Rosenbusch, J. P.; Zulauf, M.; Timmins, P. A. *Structure* **1995**, *3*, 1051.
(65) Muh, F.; Zouni, A. *Biochim. Biophys. Acta, Biomembr.* **2008**, *1778*, 2298.
(66) Ceccarelli, M.; Marchi, M. *J. Phys. Chem. B* **2003**, *107*, 1423.
(67) Fleming, K. G.; Michael, L. J.; Gary, K. A. Probing stability of helical transmembrane proteins. *Methods Enzymol.* **2000**, *323*, 63.

JP905050B